Hindawi Publishing Corporation
International Journal of Rotating Machinery
Volume 2009, Article ID 718107, 12 pages
doi:10.1155/2009/718107

Research Article

An Advanced Microturbine System with Water-Lubricated Bearings

Susumu Nakano,[1] Tadaharu Kishibe,[1] Tomoaki Inoue,[2] and Hiroyuki Shiraiwa[3]

[1] *Energy and Environmental Systems Laboratory, Hitachi Ltd., Hitachi, Ibaraki 319-1221, Japan*
[2] *Mechanical Engineering Research Laboratory, Hitachi Ltd., Hitachinaka, Ibaraki 312-0034, Japan*
[3] *Engineering Division, Hitachi Engineering & Services Co., Hitachi, Ibaraki 317-0073, Japan*

Correspondence should be addressed to Susumu Nakano, susumu.nakano.re@hitachi.com

Received 12 May 2009; Revised 16 September 2009; Accepted 24 September 2009

Recommended by Kazuhiko Kawaike

A prototype of the next-generation, high-performance microturbine system was developed for laboratory evaluation. Its unique feature is its utilization of water. Water is the lubricant for the bearings in this first reported application of water-lubricated bearings in gas turbines. Bearing losses and limitations under usage conditions were found from component tests done on the bearings and load tests done on the prototype microturbine. The rotor system using the water-lubricated bearings achieved stable rotating conditions at a rated rotational speed of 51,000 rpm. An electrical output of 135 kW with an efficiency of more than 33% was obtained. Water was also utilized to improve electrical output and efficiency through water atomizing inlet air cooling (WAC) and a humid air turbine (HAT). The operation test results for the WAC and HAT revealed the WAC and HAT operations had significant effects on both electrical output and electrical efficiency.

1. Introduction

In the USA, electricity deregulation began at the end of the 1990s. With deregulation, distributed power generation apparatuses such as microturbines were expected to play an important role. Though a booming market for microturbines was anticipated early in the 2000s, this has not realized, partially due to complicated reasons related to regulatory barriers and partially due to reasons of their low efficiencies and high costs. Gas engines have often competed against microturbines. Comparing microturbines with reciprocating gas engines reveals that the former has lower NOx emissions, lower maintenance costs, less noise, and less vibration than gas engines do. Some effort has been put into improving their efficiencies (Parente et al. [1], Williamson and Luker [2], Tsuchiya et al. [3]). The lower maintenance costs of microturbines will be of great advantage in the near future. Microturbines have an electrical efficiency of 33% to 35% and half the maintenance costs of gas engines which should make them sufficiently competitive with gas engines (Tsuchiya and Okamoto [4]).

A prototype for the next-generation microturbine system that will be able to satisfy the demand for high electrical efficiency and low maintenance costs has been developed for laboratory evaluation (Nakano et al. [5]). The final target of the present study was to develop a 150 kW machine with an electrical output efficiency of 35%, which was expected to be more competitive with gas engines. The use of water-lubricated bearings contributes to electrical output efficiency because both bearing losses and auxiliary power consumption can be reduced. Water is the lubricant for the bearings in this first reported application in gas turbines (Nakano et al. [6]). The simplified Humid Air Turbine (HAT) cycle (Hatamiya et al. [7]) was applied to achieve the target. Some calculated results and component tests on water-lubricated bearings are presented in this paper, including load tests done on the prototype microturbine with its water-lubricated bearings. The load tests were carried out with and without WAC and HAT.

2. Total Microturbine System

The regenerative Brayton cycle is usually applied to microturbines. Figure 1 is a system diagram of the microturbine used for the present study. Its main components are a single-stage centrifugal compressor, a single-stage radial turbine, a low NOx combustor, a recuperator, a permanent magnet generator, and an electrical power conversion system. The main feature of this microturbine system is its utilization of water to improve the electrical output and lubricate the bearings. Applications of WAC and HAT also improve its electrical output and electrical efficiency. The application of water-lubricated bearings reduces bearing loss. The water-circulation line and two water-supply lines for the WAC and HAT are included in the system.

The lubrication and cooling system (enclosed by the broken lines in Figure 1) consists of a motor-driven pump that circulates water in the system, a radiator for heat exchange, a circulation water tank, and a closed piping system. All water required for lubrication and cooling is supplied from the pump, and heat is eliminated by the radiator. Water from the radiator is branched into the lubrication and cooling system for the generator and the power conversion system. After lubrication and cooling, water is returned to the circulation water tank. The pressure of the feed water and return water temperature after lubrication and cooling are monitored to safeguard the microturbine.

The utilization of water for lubrication means that the oil supply unit is completely eliminated from this microturbine system. This contributes to reduced auxiliary power and maintenance costs and also contributes to increase total efficiency and electrical output for the microturbine.

3. Rotor System and Water-Lubricated Bearings

The rotor is supported by two water-lubricated bearings on each side of the permanent magnet rotor. The first is the journal bearing located on one end of the generator, and the second is the journal and thrust combined bearing located on the other side of the permanent magnet rotor which is next to the centrifugal compressor. Water-lubricated bearings are applied to simplify the microturbine system. The damping effect is larger than that for air bearings and the bearing loss is less than that for oil bearings.

The journal bearing located on one end of the generator is composed of four tilting pads as shown in Figure 2. The combined bearing which has both journal and thrust bearings in the bearing unit is shown in Figure 3. The combined bearing has a similar type of journal bearing to the one shown in Figure 2. To improve its robustness, the ten-tilting pad thrust bearing shown in Figure 3 is applied to the surface on the load side. Poly-Ether-Ether-Ketone (PEEK) plastic is used as the contact surface material for both the journal and the thrust bearings because of its superior wear resistance, good heat resistance, low friction coefficient, and sufficient strength that bearings subjected to a high-speed rotor require. In a later section, wear test results for the PEEK pads show one of the preferable characteristics for bearings that will be applied to high-speed rotors.

4. Analysis Methods

4.1. Bearing Losses. To estimate bearing losses, water film pressure distribution and temperature distribution are calculated. The governing equations are a Reynolds equation for the pressure distribution and an energy equation for the temperature distribution. The governing equations for the journal bearings with turbulent flow corrections described in (3) (Aoki and Harada [8]) are as follows:

$$\frac{\partial}{r\partial\theta}\left(\frac{h^3}{\mu}G_\theta\frac{\partial P}{r\partial\theta}\right)+\frac{\partial}{\partial Z}\left(\frac{h^3}{\mu}G_Z\frac{\partial P}{\partial Z}\right)=\frac{U}{2}\frac{\partial h}{r\partial\theta}, \tag{1}$$

$$\rho C_p\frac{Uh}{2}\frac{\partial T}{r\partial\theta}-\rho C_p\frac{h^3}{\mu}\left(G_\theta\frac{\partial P}{r\partial\theta}\frac{\partial T}{r\partial\theta}+G_Z\frac{\partial P}{\partial Z}\frac{\partial T}{\partial Z}\right)=\tau_C\frac{\mu U^2}{h}+\frac{h^3}{\mu}\left\{G_\theta\left(\frac{\partial P}{r\partial\theta}\right)^2+G_Z\left(\frac{\partial P}{\partial Z}\right)^2\right\}, \tag{2}$$

$$G_\theta=\frac{1}{12\left(1+0.00116R_h^{0.916}\right)},$$

$$G_Z=\frac{1}{12\left(1+0.0012R_h^{0.845}\right)}, \tag{3}$$

$$\tau_C=1+0.0012{R_h}^{0.94},$$

where, $R_h=U\rho h/\mu$.

The governing equations for the thrust bearing are basically the same as ones for the journal bearing. The r and Z in (1) and (2) have the same coordinate which is taken as the direction for the bearing pad width while the r means the journal radius for the journal bearings. Relationship between kinematic viscosity and temperature is expressed in (4) which is known as the Walther equation:

$$\log\log(\upsilon\times10^6+0.7)=C_1-C_2\log T. \tag{4}$$

The C_1, and C_2 are constants on the basis of water characteristics.

The governing equations are solved using a finite difference method to obtain the pressure and temperature distributions in the water film. The pressure at the periphery is assumed to be the ambient pressure. The details of the calculation procedures have been described in Suganami et al. [9] and Kaneko and Mitsuya [10].

The bearing loss caused by a pad can be calculated in (5) using the water film thickness, the pressure distribution obtained from the Reynolds equation, and viscosity obtained from (4). Total bearing losses are summation of calculation results for each pad:

$$L_{b,p}=\omega\int_{Z_1}^{Z_2}\int_{\theta_1}^{\theta_2}\left(\frac{\mu U}{h}+\frac{h}{2}\frac{\partial P}{r\partial\theta}\right)r^2\,d\theta\,dZ. \tag{5}$$

4.2. Churning Loss Caused by Rotating Thrust Collar. The friction loss caused by rotating disks cannot be disregarded when they rotate at high speed. This kind of loss is considered

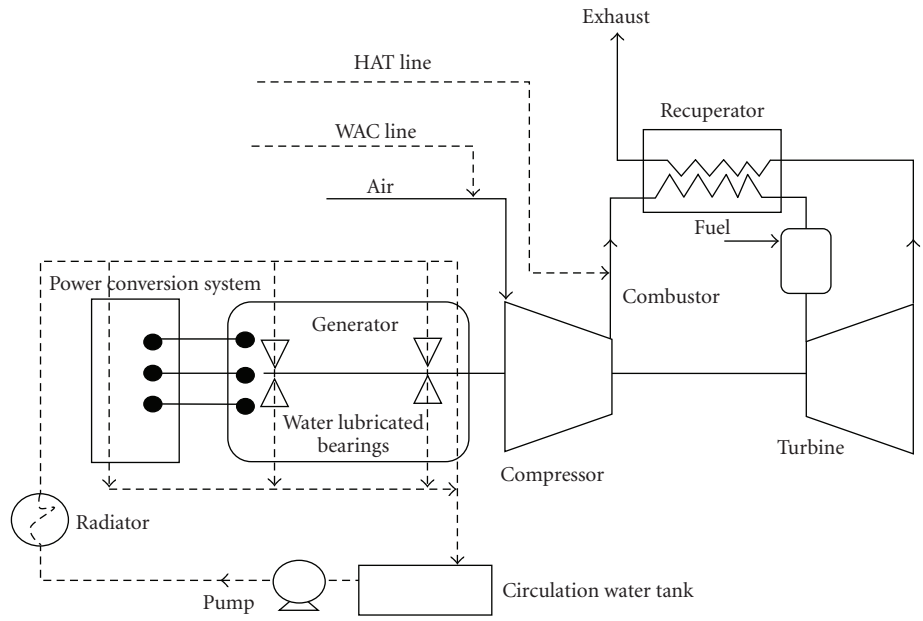

Figure 1: System diagram of microturbine using WAC and HAT.

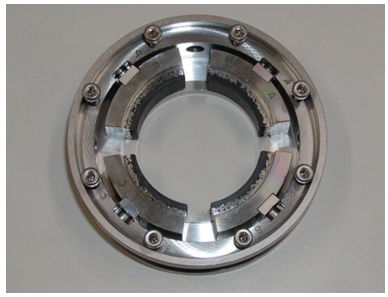

Figure 2: Journal bearing.

Figure 3: Combined bearing.

to be churning loss which occurs in the space between the tilting pads. Friction loss acting on the disk surface can be estimated by multiplying the friction force moment on the disk by the angular velocity. When the friction shear stress τ is expressed as $\xi\rho r^2\omega^2/2$, churning loss can be written as the next equation:

$$\begin{aligned} L_{\text{churn}} &= \omega M = \omega \int_{ri}^{ro} 2\pi r \frac{A_{\text{th},s} - A_{\text{th,pad}}}{A_{\text{th},s}} (\tau \cdot r) dr \\ &= \frac{A_{\text{th},s} - A_{\text{th,pad}}}{5A_{\text{th},s}} \xi\rho\pi\omega^3 \left(r_o^5 - r_i^5\right). \end{aligned} \tag{6}$$

Applying the dimensionless moment coefficient C_M which is defined by Schlichting [11], the coefficient of friction ξ in (6) is equal to $5C_M/(4\pi)$ (Senoo [12]):

$$C_M = \frac{2M}{(1/2)\rho\omega^2(r_o{}^5 - r_i{}^5)}. \tag{7}$$

So the coefficient of friction can be written by using C_M:

$$\begin{aligned} \xi &= 1.063 \left(\frac{r_0{}^2\rho\omega}{\mu}\right)^{-0.5} \quad \left(10^4 \le \frac{r_0{}^2\rho\omega}{\mu} \le 2\times 10^5\right), \\ \xi &= 0.0248 \left(\frac{r_0{}^2\rho\omega}{\mu}\right)^{-0.2} \quad \left(2\times 10^5 < \frac{r_0{}^2\rho\omega}{\mu} \le 10^7\right). \end{aligned} \tag{8}$$

When part of the thrust collar is submerged in lubricant water, friction force acts on the cylindrical surface of the thrust collar to generate loss. The loss is expressed using the area ratio $(\sigma/2\pi)$ of the immersed area to the whole circumferential area:

$$L_{\text{th},i} = \xi \frac{\sigma}{2\pi} \rho\pi\omega^3 r_o{}^4 b. \tag{9}$$

4.3. Heat Transfer Model on Bearing Surface. There are three kinds of heat that raise the temperature of the lubricant

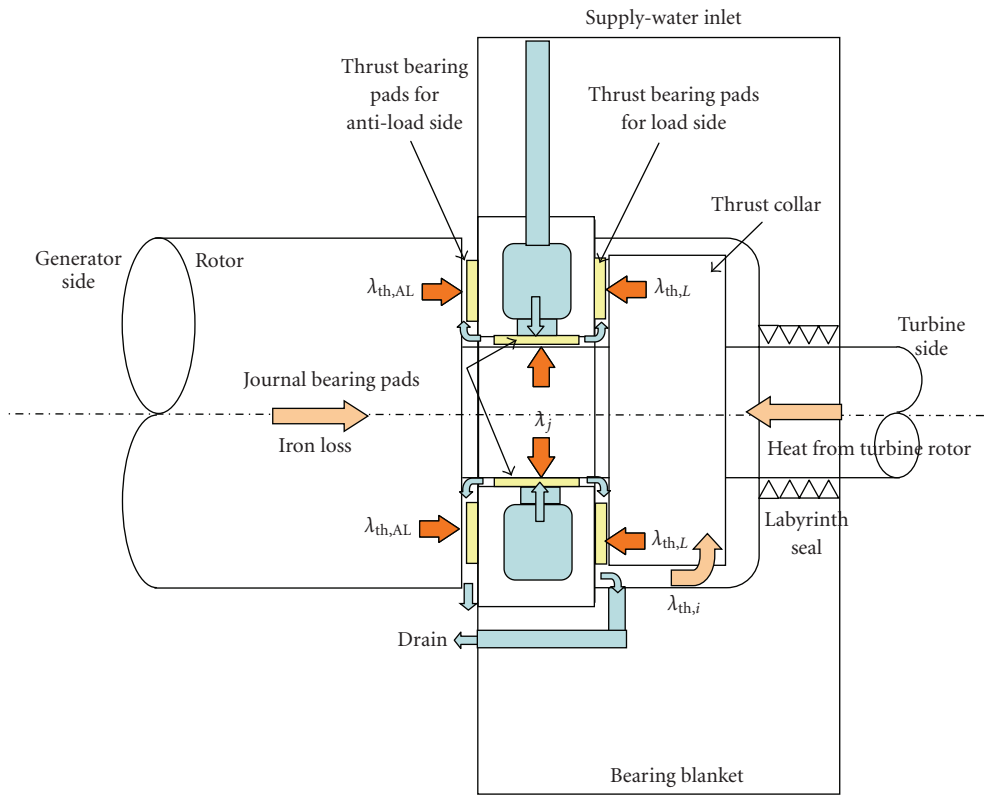

Figure 4: Heat and water flow around the combined bearing.

water. The first is heat that is generated by the bearings themselves, such as journal bearing loss, thrust bearing loss, and churning loss. The second is heat that is conducted into the rotor, such as iron loss of the generator rotor and heat from the turbine rotor. The third is heat that is generated by moving the lubricant water along the cylindrical surface of the thrust collar when part of the thrust collar is immersed in the lubricant water. This heat repenetrates into the rotor from the surface of the thrust collar.

Figure 4 is a schematic that describes the lubricant water and heat flow around the combined bearing. The lubricant water is supplied from the supply-water inlet of the bearing blanket. The supplied water first sweeps over the surface of the journal bearing pads, is split into the load side and antiload sides of the thrust bearings, and is discharged by passing through the thrust pads. Heat that has been conducted into the rotor diffuses from the three surfaces of the combined bearing; these are the surfaces of the journal bearing pads, the load side of the thrust bearing, and its antiload side. All the conducted heat is divided into heat that passes through the journal bearing surface and through the thrust bearing surface. The conducted heat is divided in proportion to the product of the heat transfer surface area and the heat transfer coefficient. The heat transfer coefficient on the cylindrical surface of the journal bearing is in proportion to the 0.7th power of the inner diameter of the journal bearing because the Nusselt number is expressed by the 0.7th power of the Reynolds number and the circumferential velocity is taken as the reference velocity of the Reynolds number. The heat transfer coefficient of the thrust bearing surfaces is similar and is in proportion to the 0.8th power of the outer diameter of the thrust bearing pads:

$$\lambda_j = \left(\frac{{d_j}^{0.7} A_{j,\mathrm{pad}}}{{d_j}^{0.7} A_{j,\mathrm{pad}} + {d_{\mathrm{th}}}^{0.8} A_{\mathrm{th,pad}}}\right)\lambda_{\mathrm{in}},$$
$$\lambda_{\mathrm{th}} = \left(\frac{{d_{\mathrm{th}}}^{0.8} A_{\mathrm{th,pad}}}{{d_j}^{0.7} A_{j,\mathrm{pad}} + {d_{\mathrm{th}}}^{0.8} A_{\mathrm{th,pad}}}\right)\lambda_{\mathrm{in}}, \tag{10}$$

$$\lambda_{\mathrm{in}} = Q\rho C\Delta T_{\mathrm{drn}} - \left(L_j + L_{\mathrm{th}} + L_{\mathrm{churn}}\right). \tag{11}$$

Considering the heat transfer on rotating disks (Owen et al. [13]), the heat transfer rates on the load and antiload sides of the thrust bearing are assumed to be in inverse proportion to the gap between the bearing pad surface and thrust collar or rotor surface. The heats transferred to each side of the thrust bearing are written as follows:

$$\lambda_{\mathrm{th},L} = \left(\frac{A_{\mathrm{th,pad},L}/G_{\mathrm{th},L}}{A_{\mathrm{th,pad},L}/G_{\mathrm{th},L} + A_{\mathrm{th,pad,AL}}/G_{\mathrm{th,AL}}}\right)\lambda_{\mathrm{th}}, \tag{12}$$

$$\lambda_{\mathrm{th,AL}} = \left(\frac{A_{\mathrm{th,pad,AL}}/G_{\mathrm{th,AL}}}{A_{\mathrm{th,pad},L}/G_{\mathrm{th},L} + A_{\mathrm{th,pad,AL}}/G_{\mathrm{th,AL}}}\right)\lambda_{\mathrm{th}}. \tag{13}$$

4.4. Temperature Rise in Lubricant Water. It is essential to estimate the temperature rise in lubricant water because its use is limited by the water boiling point. Lubricant water is divided into load and antiload sides. When the temperature rise on the load side of lubricant water is estimated, the distribution rate of supplied water into the load side and antiload side is needed. In this section, first deduction of the distribution rate is explained, and second an equation for the temperature rise on the load side of the thrust bearing is shown.

The flow rate ratio supplied to the load side and antiload side is deduced by simple equations of energy conservation along the water path. The upstream boundary is taken to be at the supply-water inlet for the journal bearing, and the downstream boundary is taken to be at the perimeter of the thrust bearing. The pressure difference between the upstream and downstream boundaries can be expressed by two energy equations that are written for each flow path on the load and antiload sides. Then, the relationship equations for flow rate are added:

$$\begin{gathered}\Delta P = \zeta_j \frac{1}{2}\rho {u_L}^2 + (\zeta_{\mathrm{th},L} + 1)\frac{1}{2}\rho {v_L}^2,\\ \Delta P = \zeta_j \frac{1}{2}\rho {u_{\mathrm{AL}}}^2 + (\zeta_{\mathrm{th,AL}} + 1)\frac{1}{2}\rho {v_{\mathrm{AL}}}^2,\\ u_L = \frac{A_L}{A_J} v_L,\\ u_{\mathrm{AL}} = \frac{A_{\mathrm{AL}}}{A_J} v_{\mathrm{AL}} = \frac{Q - A_L v_L}{A_J},\\ v_{\mathrm{AL}} = \frac{Q - A_L v_L}{A_{\mathrm{AL}}}.\end{gathered} \tag{14}$$

The flow rate ratio of the water supplied to the load and antiload sides is derived by (15). Even though a precise value for the flow rate ratio of lubricant water cannot be calculated without accurate values for pressure loss coefficients, the relationships between flow rate ratios, cross-sectional area ratios, and friction coefficient ratios can be found:

$$\frac{Q_L}{Q_{\mathrm{AL}}} = \frac{-({a_1}^2 + a_2{}^2\zeta_2) \mp \sqrt{({a_1}^2 + a_2{}^2\zeta_2)({a_1}^2 + \zeta_1)}}{({a_1}^2 + \zeta_1) \pm \sqrt{({a_1}^2 + a_2{}^2\zeta_2)({a_1}^2 + \zeta_1)}}, \tag{15}$$

$$\begin{gathered}a_1 = \frac{A_L}{A_J},\\ a_2 = \frac{A_L}{A_{\mathrm{AL}}},\\ \zeta_1 = \frac{\zeta_{\mathrm{th},L} + 1}{\zeta_j},\\ \zeta_2 = \frac{\zeta_{\mathrm{th,AL}} + 1}{\zeta_j}.\end{gathered} \tag{16}$$

Though ζ_1 and ζ_2 are included as unknown parameters, the flow rate ratio described in (15) can be expressed by the cross-sectional area ratios of the lubricant water flow passes. Effects of ζ_1 and ζ_2 for the flow rate ratio can be shown by calculating (15) for various values of ζ_1 and ζ_2. The distribution rate is defined by

$$\alpha = \frac{1}{1 + Q_{\mathrm{AL}}/Q_L}. \tag{17}$$

The temperature rise of lubricant water passed through the load side of the thrust bearing is expressed by using the distribution rate in (17). Once the distribution rate is determined, the temperature rise of lubricant water passed through the load side of the thrust bearing can be estimated easily:

$$\Delta T_L = \frac{(L_{\mathrm{th}} + \lambda_{\mathrm{th},L}) + \alpha\left(L_j + \lambda_j\right)}{\alpha C Q \rho}. \tag{18}$$

On the other hand, if the temperature rise in lubricant water that has passed through the load side of the thrust bearing can be measured, the distribution rate is given by

$$\alpha = \frac{(L_{\mathrm{th}} + \lambda_{\mathrm{th},L})}{CQ\rho\Delta T_L - \left(L_j + \lambda_j\right)}. \tag{19}$$

Though it is difficult to measure the temperature rise in lubricant water that has passed through the load side of the thrust bearing in the prototype microturbine, it can be measured in the component test of the generator test because the test rigs are configured to allow easy measurement of the temperature.

4.5. Calculation of Thrust Load. Thrust load is also monitored during microturbine operation. The inlet and exit static pressures of the centrifugal compressor impeller and the turbine rotor, and the static pressure of the back and forth labyrinth seal, which is located between the compressor and turbine, are measured to calculate thrust load. Thrust load can be calculated assuming that the hub surface and back surface of the impellers have static pressure profiles. The static pressure profiles are presumed to be a squared function of the radius based on the Euler equation. The static pressure profile is obtained as (20) using measurements of inlet and exit static pressures:

$$P = P_i + \frac{(P_o - P_i)}{({r_o}^2 - {r_i}^2)}(r^2 - {r_i}^2). \tag{20}$$

Thrust load is calculated as the balance of forces acting on the compressor impeller and turbine rotor. Each force acting on the hub or back surfaces is given by

$$F = 2\pi \int_{r_i}^{r_o} rP dr. \tag{21}$$

The total thrust loading on the rotor system can be deduced by adding both forces acting on the end surfaces of the generator rotor.

5. Experimental Apparatuses

Three kinds of experimental apparatuses are used to test and confirm the characteristics of the water-lubricated bearings. All three are described here.

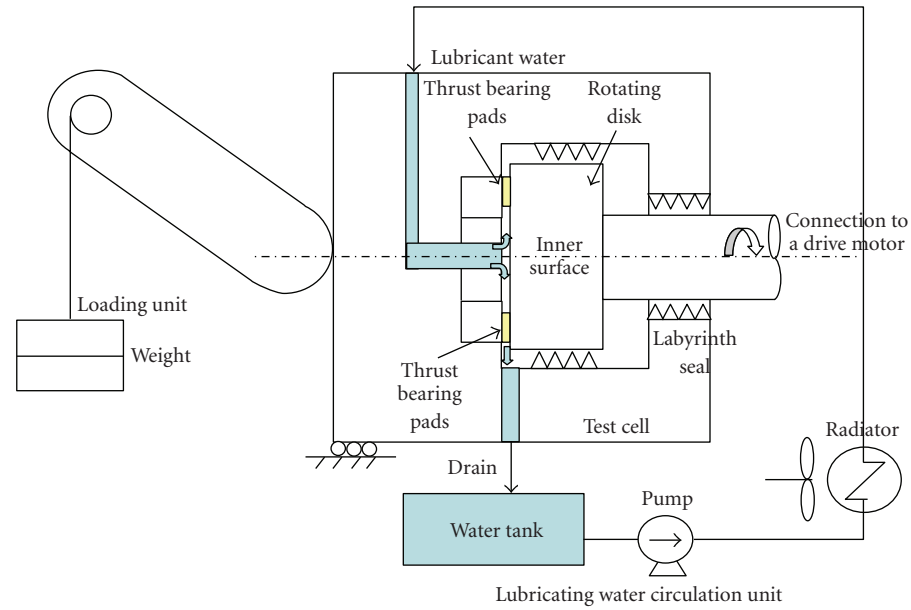

Figure 5: Schematic of thrust bearing test rig.

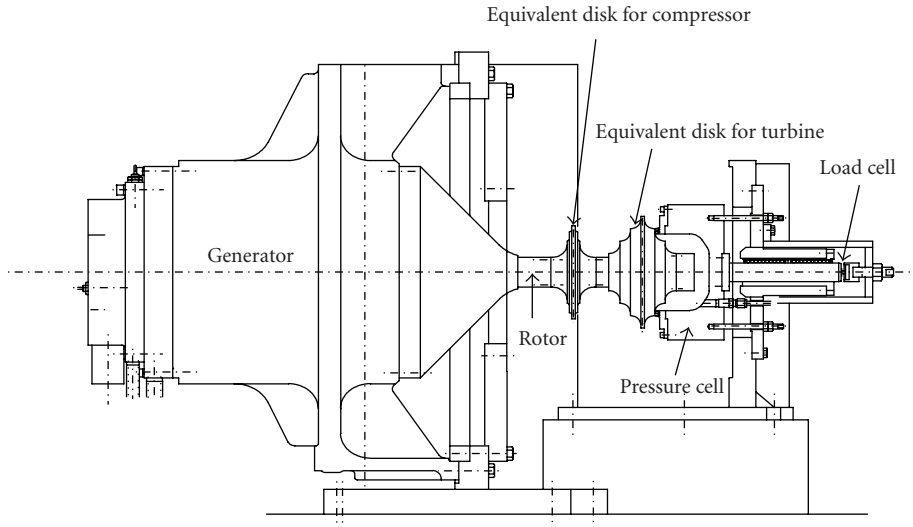

Figure 6: Generator test setup.

5.1. Component Test Rig for Bearings. Component tests on the bearings are done to confirm bearing losses, limitations on the temperature rises in lubricant water and their characteristics against resistance to wear. Figure 5 shows the component-testing rig for the thrust bearing. The test rig is composed of a driving motor, a rotating disk, a test cell for the bearing, a loading unit, and a lubricant water circulation unit into which a pump, radiator, and water tank have been assembled. The rotating speed can be increased up to 51,000 rpm. The thrust load can be varied to 540 N by changing the weight of the loading unit. The temperature of the supply water can be changed to control the air flow rate passing through the radiator.

5.2. Generator Test Rigs. Figure 6 shows the rig used to test the generator. This test rig is primarily used to measure the electrical characteristics of the generators for the microturbine. Even though the generator used in the bearing tests is the same as the one applied in the microturbine, the generator rotor used in the tests is simulated so that the mass and inertia are equal. The impellers for the compressor and turbine rotor are formed on equivalent disks to reduce the windage.

This test rig applies thrust load on the generator rotor. A pressure cell is located on one side of the equivalent disk of the turbine rotor and is pressurized by compressed air blown into the pressure cell. Load acting on the pressure cell

Figure 7: Photograph showing one side of the prototype microturbine system.

is measured with a load cell located on the other side of the pressure cell, and this is equal to thrust load acting on the thrust bearing.

5.3. Microturbine Prototype. Finally, the bearings that have been developed are installed in the prototype microturbine. Figure 7 is a photograph of one side of the prototype, which is completely packaged. The main components are on the upper floor of the package. The power conversion system is under the floor. There is a radiator fan to eliminate the heat of the circulation water and to ventilate the room downstream from the power conversion system.

6. Results of Calculation and Component Tests

6.1. Results of Calculation of Bearing Losses. The calculated results are plotted in Figure 8. The journal bearing losses do not depend on thrust load and can be described in one curve. They are about 1.25 kW at the rated rotational speed. The thrust bearing losses are directly affected by thrust load and vary from 0.8 kW to 2.5 kW at the rated rotational speed corresponding to thrust load from 100 to 1,000 N. Figure 9 plots the calculated results for water film thickness, which is needed to estimate the heat transfer rate of the thrust bearings, given in (11) and (12), and also needed in the calculations for the distribution ratio because the a_2 in (15) is determined by the water film thickness which depends on thrust load.

6.2. Calculated Results for Churning Loss of Thrust Bearing. Figure 10 plots the calculated results for (6) and (9). At the rated speed of 51,000 rpm, churning loss reaches about 0.8 kW. The friction loss acting on the cylindrical surface of the thrust collar is larger than the churning loss. The

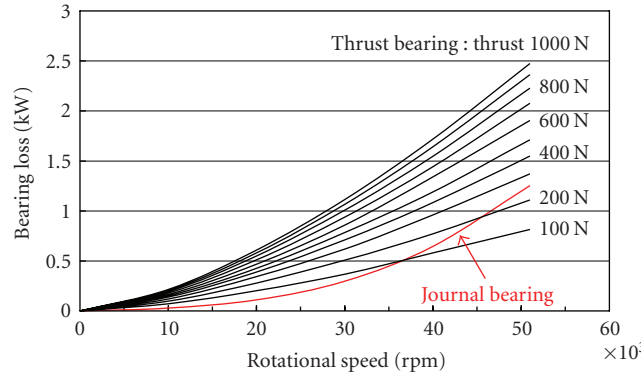

Figure 8: Calculated results for bearing losses.

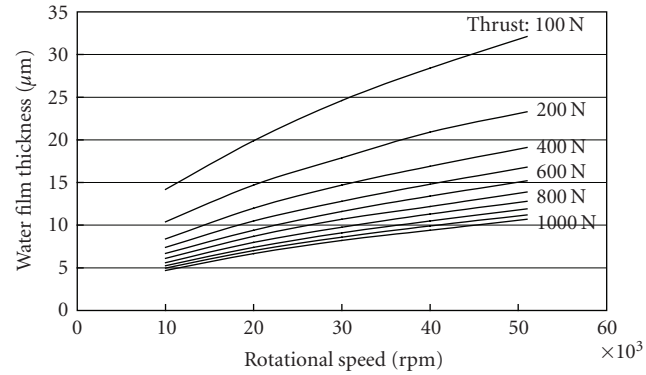

Figure 9: Calculated results for water film thickness.

bluish-purple line in Figure 10 represents the calculated results obtained by (9) at $\sigma = 0.3\pi$, where 15% of the cylindrical surface has been assumed to have been immersed into lubricant water. When the supply of lubricant water increases, the cylindrical surface appears to be immersed in the lubricant water. Even though it is easy to surmise that increased friction loss is generated by the cylindrical surface of the rotor when more water is supplied, it is difficult to accurately calculate the area that is immersed in the lubricant water because the immersed area of the cylindrical surface strongly depends on the supply-water rate and the structure of the bearing, the blanket, and the inlet and outlet for the lubricant water. It is important not to immerse the cylindrical surface of the rotor when the flow rate of the lubricant water is increased. Once part of the cylindrical surface of the rotor is immersed in lubricant water, the cylindrical surface friction loss which is more than the disk friction loss will be generated.

6.3. Results for Bearing Component Tests. Figure 11 plots the total bearing losses measured through temperature rises in the lubricant water that has passed through the thrust bearing. The calculated results for the thrust bearing that were given in Figure 8 have been added to Figure 11. The total loss and calculated results increase with thrust load. The difference between the total loss and calculated results seems to be churning loss in the thrust bearing because churning

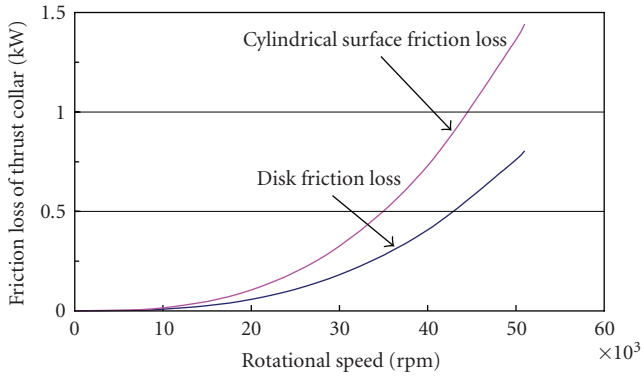

Figure 10: Calculated results for friction losses of thrust collar.

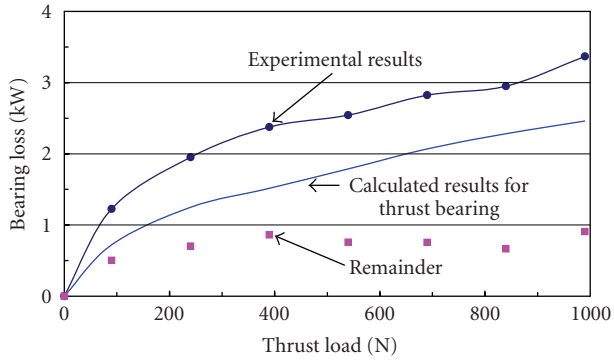

Figure 11: Results for bearing component tests.

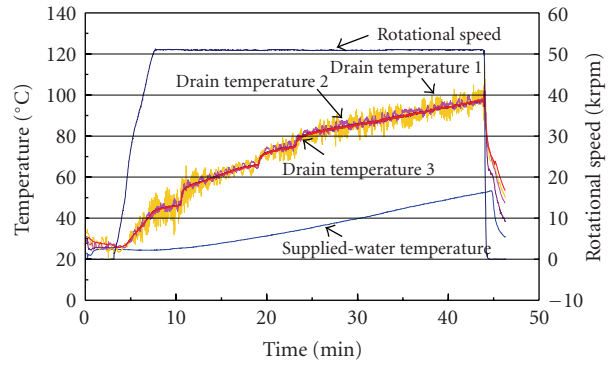

Figure 12: Experimental results for temperature rise in lubricant water through thrust pads.

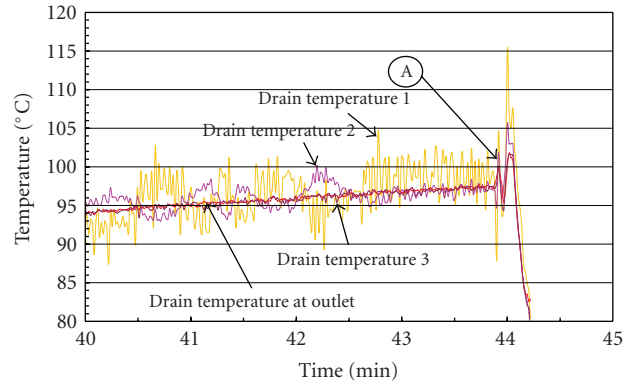

Figure 13: Expanded scale plot of temperature rises in lubricant water.

loss does not depend on thrust load and the remainder is almost constant toward thrust load. Even though the remainder of about 0.8 kW corresponds to the results in Figure 10, it should include friction loss that is generated on the inner surface of the rotating disk. The friction loss reaches 0.3 kW using a similar calculation with (6). Therefore, the churning loss is thought to be about 0.5 kW.

Figure 12 plots the temperatures of the supply and drain water for the thrust bearing. The temperatures of the drain water are measured at three points close to the outer circumference of the thrust bearing pads. The maximum thrust load of 540 N acts on the bearing surface for 23 minutes. The drain-water temperatures at the three points gradually rise. After 44 minutes, the drain temperatures reach the boiling point and the thrust bearing pads are severely damaged.

Figure 13 uses an expanded scale to plot the drain temperatures at around 44 minutes. Drain temperature 1 frequently exceeds 100°C after 40 minutes. At about 44 minutes, all temperatures at the three points exceed 100°C. Point A in Figure 13 is the point at which the bearing broke. The average pressure on the water film is about 490 kPa when a thrust load of 540 N acts on it. Even though the boiling temperature at 490 kPa is about 150°C, the thrust bearing cannot sustain the thrust load and it is severely damaged. Even though the lubricant water does not exceed the boiling point of 150°C on the periphery of the pads, it is exposed to atmospheric pressure and the water boils. The bubbles that are generated on the periphery of the pads are thought to affect the wedge-shaped water film that had formed between the pads and the rotating disk, which can sustain thrust load.

6.4. Results for Generator Tests. The generator test results are plotted in Figure 14. The tests are done for a rated rotational speed of 51,000 rpm. The bearing losses are calculated using the temperature rise in the lubricant water. The total loss includes both journal and thrust losses. The calculated results for the journal and thrust losses under all experimental thrust load conditions are also plotted in Figure 14. The difference between the total loss and the sum of the calculated losses is about 0.7 kW under all thrust load conditions. These differences are thought to be caused by the churning loss in the water and the iron loss of the generator rotor with no load. These losses depend on the rotational speed and do not depend on thrust load.

Comparing the remainder in Figure 14 to that in Figure 11 shows that they both are almost the same. As previously mentioned, the results in Figure 11 include the extra friction loss that was generated by the inner area of the rotating disk. It is clear that the bearing component test shown in Figure 11 does not include iron loss and the results in Figure 14 must include it. Consequently, the iron loss of the generator rotor is thought to be about 0.2 kW.

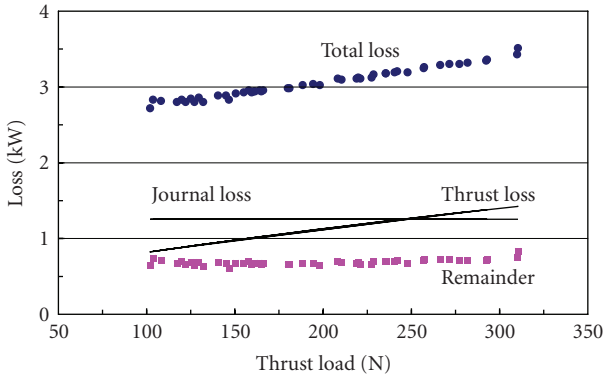

Figure 14: Results of the generator test.

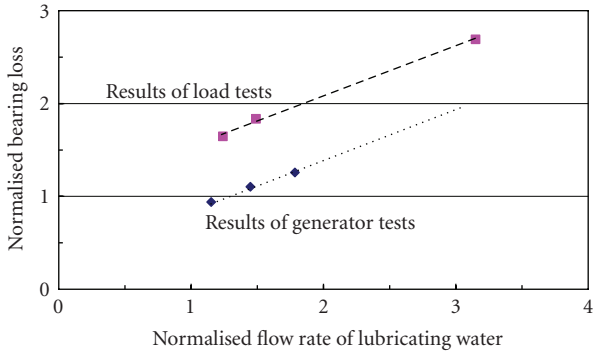

Figure 15: Effects of flow rate of lubricant water.

Figure 15 plots the effect of the flow rate of supply water. An increase in the flow rate of the supply water causes friction losses by the thrust collar, and the cylindrical surface of the thrust collar especially has the potential for generating friction losses larger than the churning loss. The experimental conditions except for the flow rate of the supply water are the same; the generator rotor acts on about 100 N of thrust load, which was generated by magnetic pull. The x-axis shows the normalized flow rate for the lubricant water, which is specified by a flow rate that enables a temperature rise of 40°C for the 200 N thrust load conditions. The y-axis shows the normalized bearing loss, which is calculated by adding the journal bearing loss at the rated speed, the thrust bearing loss for a thrust load of 200 N, and a churning loss of 0.5 kW. The results for the load test on the prototype microturbine are also plotted in the figure. The rate of increased bearing loss is the same, and it is obvious that the increase in flow rate of lubricant water affects the increase in bearing loss. The difference between the results for the load tests and generator tests is about 0.55, and this seems to be caused by conduction heat transfer from the turbine rotor.

Figure 16 plots the calculated distribution rates. The a_2 term in (15) is determined as the ratio between the water film thickness and the value subtracting the water film thickness from the total thrust gap. As shown in Figure 9, water film thickness was affected by thrust load. So the distribution ratio is also affected by thrust load. The distribution rates decrease when the loss coefficient on the load side of the

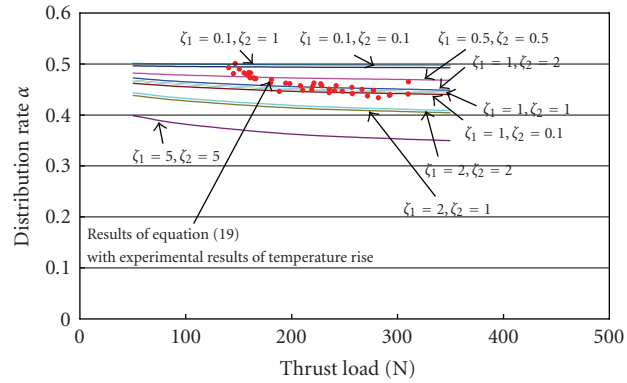

Figure 16: Comparison of distribution rates.

thrust bearing increases, and they decrease when the loss coefficient on the antiload side of the thrust bearing decreases with the constant loss coefficient on the load side of the thrust bearing. These results do not contradict intuition. The a_2 term is a more prevailing parameter for the distribution rate than the a_1 term.

The results calculated with (19) using the experimental values for temperature rise are also plotted. Though the distribution rate for the load side of the thrust bearing decreases when thrust load increases, both results of calculations and experiments do not show a large change toward the thrust load. An α of 0.45 is recommended for the thrust bearing calculations.

6.5. Results of Wear Test for PEEK Pads of Thrust Bearings. Lastly, to confirm the lifetime of PEEK plastic pads under actual operating conditions, a wear test is conducted with the component test rig for bearings taking the start-up conditions of operation into consideration. Wear is thought to be generated under boundary-lubrication conditions, while a complete water film is formed at a rotational speed of 3,000 rpm. As a result, a rotational speed of 1,500 rpm is selected for the rotating disk. Figure 17 plots the results for the wear test. About 7 μm of wear occurs after the 50 hours of operation. These 50 hours correspond to 100,000 start-up and shutdown times. PEEK plastic pads have a sufficiently long lifetime for microturbine operation.

7. Results for Load Tests of Microturbine

7.1. Temperature Rise in Lubricant Water for the Combined Bearing. Figure 18 plots the calculated results for temperature rise in lubricant water and normalized bearing loss for the prototype microturbine. The thrust load is assumed to be 200 N. The plotted lines indicate design specifications for the water-lubricated bearing. First, the flow rate for the supply water is determined to maintain the temperature rise in the lubricant water under 40°C. That means the normalized flow rate is equal to 1. The temperature rise in the lubricant water passing through the load side of the thrust bearing is higher than that of drain water. The heat transfer rate can be calculated from (12) and (13) using the water film thickness

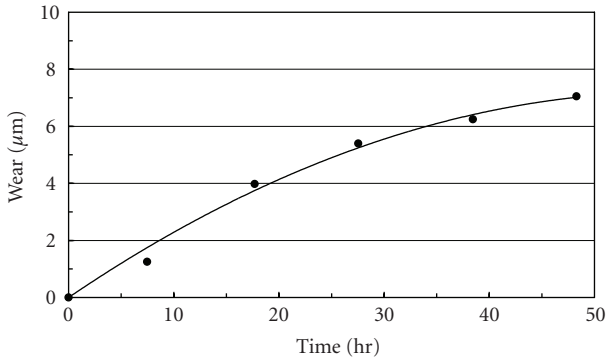

Figure 17: Results of wear test for PEEK pads.

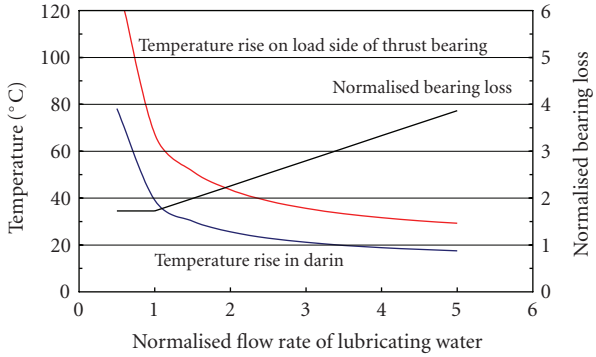

Figure 18: Relationship between temperature rise in lubricant water and bearing loss.

given in Figure 9. The distribution rate here is assumed to be 0.45, the temperature rise on the load side of the thrust bearing reaches 70°C under thrust load conditions of 200 N, and conducted heat from the turbine rotor is 1.7 kW. To keep the temperature under 40°C, the flow rate of the lubricant water has to be doubled. This increases bearing loss. An appropriate balance point for temperature rise and bearing loss has to be determined under the prototype microturbine operating conditions.

Figure 19 plots the calculated results for water temperature on the load side of the thrust bearing using (18) for the load tests on the prototype microturbine. The dashed line indicates the boiling temperature at atmospheric pressure, the open diamonds indicate the results of normal operation with a normalized flow rate of 1, and the open circles indicate the results of normal operation with a normalized flow rate of 1.5. The three closed triangles above the boiling temperature line indicate failed operation with a normalized flow rate of 1. These operations brought severe damage to the bearings in the load tests.

7.2. Results for Load Tests. The rotor has a natural frequency in the first bending mode around 22,000 rpm. Stable operation is obtained from the start to the rated speed of 51,000 rpm. The vibration amplitude at the rated speed is under 20 μm.

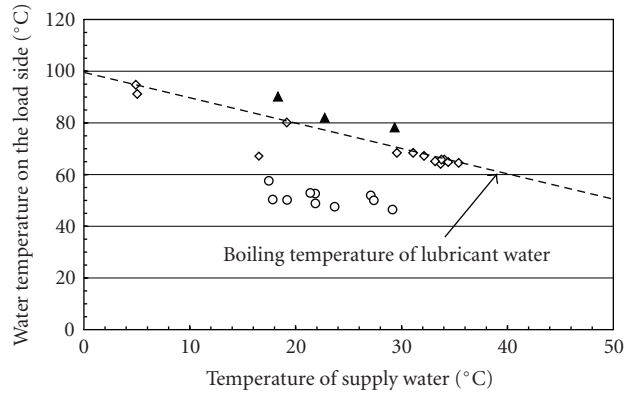

Figure 19: Water temperature calculated with (18) using results of load tests for prototype microturbine.

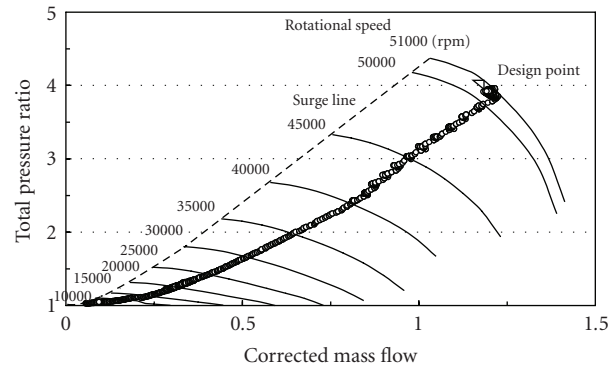

Figure 20: Running curve for rated load tests without WAC and HAT.

Figure 20 plots the running curve for rated load. The x-axis represents the corrected mass flow rate. It can be seen that there is enough margin for the surge line and the design point of the pressure ratio is almost reached at the rated rotational speed. An electrical output of 135 kW with an electrical efficiency of 33.2% is obtained on the grid side. The electrical output on the grid side is the output power which is subtracted the auxiliary power from the output power of the power conversion system, and the electrical efficiency on the grid side is also considered the auxiliary power. The main auxiliary power includes the power for the water circulation pump, the radiator fan, the rotor cooling blower, and the plunger pump for the WAC and HAT.

The operation tests for WAC and HAT are carried out under 63% load condition in a preliminary test. The water flow rate for the WAC is 4.5 g/s, and that for the HAT is 21 g/s. The auxiliary power jumps from 2.6 kW to 4.7 kW when the plunger pump starts to work.

Figure 21 shows the change in electrical output when the WAC and HAT operations are carried out. The effects of WAC and HAT are immediately reflected in the electrical power with almost no delay. The electrical efficiency has the same trend as the electrical output when the WAC and HAT operations are undertaken. When the WAC is

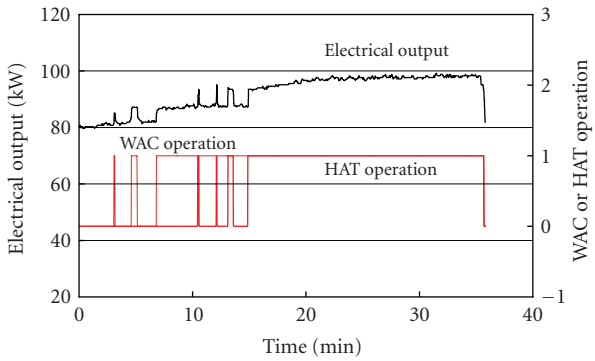

Figure 21: Electrical output during WAC and HAT operations.

operated, the electrical output increases about 6 kW and the efficiency increases 1.0%. When the HAT operation is added, the electrical output increases about 11 kW and efficiency increases 2.0%. The total improvement amounts to a 17 kW increase in electrical output with a 3.0% increase in electrical efficiency. No drain water is captured in the drain pipe.

8. Conclusions

A prototype of the next-generation microturbine system applying a simple humid air turbine cycle was developed for laboratory evaluation.

(1) Water-lubricated bearings were developed for the prototype and this was their first application in gas turbines.

(2) Bearing losses and limitations under usage conditions were established as results of component tests done on the bearings and load tests on the prototype microturbine.

(3) The rotor system using the water-lubricated bearings achieved stable rotating conditions at a rated rotational speed of 51,000 rpm.

(4) Rated load tests without WAC and HAT were successfully completed and an electrical output of 135 kW with an efficiency of 33.2% was achieved.

(5) The operation tests on WAC and HAT, which were carried out under a load of 63%, revealed that the WAC and HAT operation had significant effects on increased electrical efficiency (3.0%) and electrical output (20%).

Nomenclature

A_{AL}: Cross-sectional area of flow path for antiload side of thrust bearing (m^2)
A_J: Cross-sectional area of flow path for journal bearing (m^2)
$A_{j,pad}$: Surface area of journal bearing pads (m^2)
A_L: Cross-sectional area of flow path for load side of thrust bearing (m^2)
$A_{th,pad}$: Surface area of thrust bearing pads (m^2)
$A_{th,s}$: Disk surface area of thrust collar (m^2)
b: Width of thrust collar (m^2)
C: Specific heat of water (J/kg/K)
C_p: Specific heat at constant pressure (J/kg/K)
d: Diameter (m)
F: Force acting on impellor or rotor (N)
G: Gap (m)
h: Water film thickness (m)
$L_{b,p}$: Bearing loss for one pad (W)
L_j: Journal bearing loss (W)
L_{churn}: Churning loss (W)
L_{th}: Thrust bearing loss (W)
$L_{th,i}$: Friction loss generated by immersed thrust collar (W)
M: Moment of friction force (Nm)
P: Pressure (Pa)
ΔP: Pressure difference (Pa)
Q: Flow rate of lubricant water (m^3/s)
T: Temperature (K)
ΔT: Temperature rise (K)
ΔT_{drn}: Temperature rise in drain (K)
U: Circumferential velocity (m/s)
u: Passage velocity of water at A_j (m/s)
v: Passage velocity of water at A_L or A_{AL} (m/s)
r, θ, Z: Cylindrical coordinates for bearing pad (m)
θ_1, θ_2: Integral range of rotational direction of a bearing pad (m)
Z_1, Z_2: Integral range of width direction of a bearing pad (m)
α: Distribution ratio of lubricant water (−)
λ_{in}: Total heat transferred to both journal and thrust bearings (W)
λ_j: Heat transferred to journal bearing (W)
λ_{th}: Heat transferred to thrust bearing (W)
μ: Viscosity (Pa s)
υ: Kinematic viscosity (m^2/s)
ρ: Density (kg/m^3)
σ: Area ratio of thrust collar immersed in water (−)
τ: Friction shear stress (N/m^2)
ω: Rotational velocity (rad/s)
ξ, ζ: Coefficient of friction (−).

Subscripts

AL: Antiload side of thrust bearing
i: Inner
J, j: Journal bearing
L: Load side of thrust bearing
o: Outer
th: Thrust bearing.

Acknowledgments

This research was supported in part by a Grant from the New Energy and Industrial Technology Development Organization (NEDO), Japan. The authors wish to express their gratitude to NEDO for its generous support.

References

[1] J. Parente, A. Traverso, and A. F. Massardo, "Micro humid air cycle part A: thermodynamic and technical aspects," in *Proceedings of the ASME Turbo Expo*, Atlanta, Ga, USA, June 2003, GT-2003-38326.

[2] T. Williamson and M. Luker, "Microturbine performance improvement though the implementation of inlet air cooling," in *Proceedings of the ASME Turbo Expo*, Reno-Tahoe, Neb, USA, June 2005, GT2005-68377.

[3] T. Tsuchiya, H. Sotouchi, T. Kubota, and K. Mochizuki, "Improvement of micro gas turbine performance by steam injection—verification of the steam injection effect and stable operation," in *Proceedings of the Asian Congress on Gas Turbines*, Seoul, South Korea, November 2005, ACGT2005-068.

[4] T. Tsuchiya and M. Okamoto, "Evaluation on the economical competitiveness of micro gas turbine cogeneration system based on efficiency and maintenance coat," in *Proceedings of the Asian Congress on Gas Turbines*, Seoul, South Korea, November 2005, ACGT2005-078.

[5] S. Nakano, T. Kishibe, and H. Araki, "Development of a 150 kW microturbine system which applies the humid air turbine cycle," in *Proceedings of the ASME Turbo Expo*, Montreal, Canada, May 2007, GT2007-28192.

[6] S. Nakano, et al., "An advanced microturbine system with water lubricated bearings," in *Proceedings of the 12th International Symposium on Transport Phenomena and Dynamics of Rotating Machinery*, Honolulu, Hawaii, USA, August 2008, ISROMAC12-2008-20185.

[7] S. Hatamiya, K. Sagae, and N. Seiki, "AHAT: gas turbine power generation technology using high humidity air," in *Proceedings of the International Conference on Power Engineering*, vol. 2, pp. 1–6, Kobe, Japan, 2003.

[8] H. Aoki and M. Harada, "Turbulent lubrication theory for full journal bearings," *Journal of Japan Society of Lubrication Engineers*, vol. 16, no. 5, pp. 348–356, 1971 (Japanese).

[9] T. Suganami, et al., "An analysis of high-speed journal bearing performance," *Journal of Japan Society of Lubrication Engineers*, vol. 25, no. 9, pp. 607–612, 1980 (Japanese).

[10] R. Kaneko and Y. Mitsuya, "Numerical analysis in fluid film lubrication," *Journal of Japan Society of Lubrication Engineers*, vol. 20, no. 12, pp. 883–889, 1974 (Japanese).

[11] H. Schlichting, *Boundary Layer Theory*, McGraw Hill, New York, NY, USA, 6th edition, 1968.

[12] Y. Senoo, *Inner Flow and Fluid Machinery*, Yokendo, Tokyo, Japan, 1973.

[13] J. M. Owen, C. M. Haynes, and F. J. Bayley, "Heat transfer from an air-cooled rotating disk," *Proceedings of the Royal Society of London. Series A*, vol. 336, no. 1607, pp. 453–473, 1974.